AGU PUBLICATIONS

Radio Science

RESEARCH ARTICLE
10.1002/2014RS005645

Key Points:
- New exact analytical solutions to two problems in EM well logging
- Derivation of new exact solutions to two fundamental problems in EM research

Correspondence to:
R. Freedman,
freedman1@slb.com

Citation:
Freedman, R. (2015), Derivation of magnetic fields on a metal cylinder excited by longitudinal and transverse magnetic dipole transmitters: I. Cylinder in unbounded dissipative dielectric medium, *Radio Sci.*, *50*, 941–955, doi:10.1002/2014RS005645.

Received 5 JAN 2015
Accepted 25 AUG 2015
Accepted article online 8 OCT 2015
Corrected 8 OCT 2015
Published online 30 SEP 2015

This article was corrected on 08 OCT 2015. See the end of the full text for details.

Derivation of magnetic fields on a metal cylinder excited by longitudinal and transverse magnetic dipole transmitters: I. Cylinder in unbounded dissipative dielectric medium

Robert Freedman[1]

[1]Schlumberger, Sugar Land, Texas, USA

Abstract We derive new and exact analytical and convergent integral representations for the frequency-dependent complex magnetic fields $H_z(a, \phi, z)$ and $H_\phi(a, \phi, z)$ excited by oscillating point magnetic dipole transmitters on the surface of an infinitely long metal cylinder of radius a in an unbounded dissipative dielectric medium. $H_z(a, \phi, z)$ is calculated for a longitudinally oriented magnetic dipole parallel to the cylinder axis and $H_\phi(a, \phi, z)$ for a transversely oriented magnetic dipole perpendicular to the axis. The solutions are relevant to the computation of phase shifts and attenuations measured by electromagnetic propagation logging tools, which have oscillating longitudinal and transverse magnetic dipole transmitters either on a metal drill collar or on a cylindrical antenna pad. The integral representations can be readily evaluated using simple numerical integration algorithms, e.g., Simpson's rule, to accurately compute the complex magnetic fields on the cylinder surface. A second paper will address the two-layer cylindrical media problem.

1. Introduction

This paper derives exact numerically convergent integrals for magnetic fields on the surface of an infinitely long metal cylinder where the magnetic fields are excited by oscillating point magnetic dipole transmitters situated on the cylinder surface. The cylinder is assumed to be perfectly conducting and is embedded in an unbounded and dissipative (i.e., conductive) dielectric medium. The two cases considered, which have theoretical and practical interest, are defined by longitudinal and transverse orientations of the magnetic dipole transmitters with respect to the cylinder axis which lies along the z axis. In a cylindrical coordinate system (r, ϕ, z) the dipoles are located on the cylinder at $(a, 0, 0)$, where a is the radius of the cylinder. The longitudinal dipole is in the z direction, and the transverse dipole is in the ϕ direction. For longitudinal and transverse dipoles, we derive numerically convergent integrals for the respective complex phasor magnetic fields $H_z(a, \phi, z)$ and $H_\phi(a, \phi, z)$ on the cylinder surface. The theoretical model for the transversely oriented dipole is shown in Figure 1. The model for the longitudinal dipole is identical except that the dipole is oriented along the z axis.

These new theoretical results are relevant to predicting the responses of electromagnetic (EM) propagation well logging tools that are used to measure the EM properties of porous rock formations penetrated by a borehole. These devices employ one or more magnetic dipole transmitters that excite EM waves which propagate in the porous fluid-filled rock formations near the borehole wall. The transmitters and multiple receivers are either situated on a drill collar or on a cylindrical antenna pad that is pressed against the borehole wall during the measurements. The phase shifts and attenuations of the EM waves propagating in the formation are measured between pairs of receivers that are longitudinally displaced from the transmitters. The measured phase shifts and attenuations are input into a model for the tool and formation to predict the conductivities and dielectric constants of the rock formations surrounding the borehole. The conductivities and dielectric constants can be used to predict the types and volumes of fluids (water, oil, and gas) in the pore spaces.

Previously published analytical models for EM propagation logging tools are based on planar models for which the transmitting and receiving antennas are situated on an infinite metallic ground plane rather than on a cylindrical antenna pad [*Freedman and Vogiatzis*, 1979; *Chew and Gianzero*, 1981; *Chew*, 1988; *Sayfina et al.*, 1987]. These papers considered a tool operating at 1.1 GHz for which the effects of the cylinder curvature are small and could be neglected. At lower transmitter frequencies the effects of pad curvature cannot

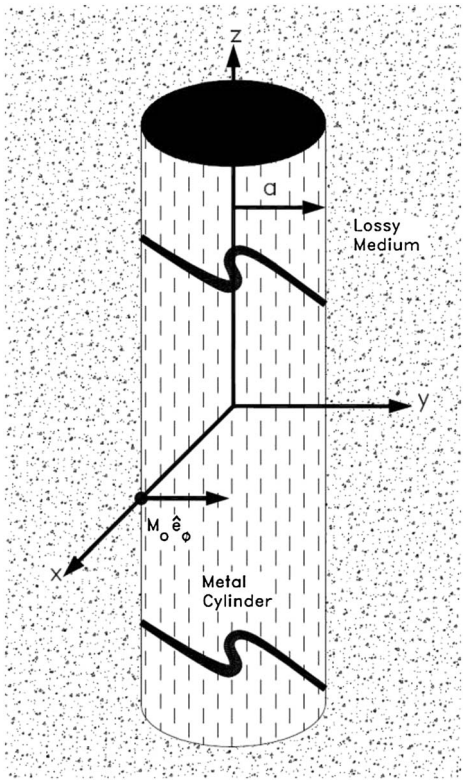

Figure 1. Schematic of the theoretical model for a transversely oriented point magnetic dipole transmitter located on the cylinder surface at (*a*,0,0). The metallic cylinder is in an unbounded dissipative dielectric medium. The theoretical model for a longitudinally oriented magnetic dipole transmitter is identical except that the transmitter magnetic moment is in the *z* direction.

be neglected. The calculation of the magnetic field everywhere on a metal cylinder is more complex than calculations for a planar model. One difficulty is that the real axis integrals for the magnetic field on the cylinder involve sums over all orders of Bessel functions with complex arguments. Moreover, the integrands are oscillatory and poorly convergent. *Wait* [1987] considered the microwave dielectric logging problem and the calculation of the magnetic fields produced by a slot antenna on a perfectly conducting infinitely long cylinder situated in a medium with an arbitrary number of cylindrical layers. Wait derived a formal solution in terms of poorly convergent real axis Fourier integrals. Wait's paper, however, did not go beyond these formal solutions, and it did not provide computable solutions that can be used for practical applications.

We show that the oscillatory and poorly convergent integrands of the real axis integrals for the magnetic fields can be replaced by branch line integrals with integrands that are smooth functions that go to zero exponentially for large values of a dimensionless integration variable. Moreover, we show that the integrands of the branch line integrals can be expressed in terms of sums over the orders of Hankel functions with real arguments that can be accurately evaluated using numerical integration. For the unbounded medium considered in this paper, no bound states or guided modes can exist so that the real axis integrals have only branch point singularities except for poles that are on the unphysical Riemann sheet in the complex integration plane.

Section 2 derives an exact convergent integral solution for $H_z(a, \phi, z)$. Section 3 derives an exact convergent integral solution for $H_\phi(a, \phi, z)$. These two solutions are displayed in equations (32) and (84), respectively, and are the main results of this paper.

The author has used the magnetic fields derived in this paper to compute differential phase shifts and attenuations for a 1.1 GHz logging tool [*Freedman*, 1992]; however, the discussion of EM well logging applications is not the purpose of this paper. This paper presents original and detailed calculations used to derive computable solutions to two important EM problems. The results presented here should be of interest to many scientists and engineers working on EM problems in academic, industrial, and military research centers.

2. Longitudinally Oriented Magnetic Dipole Transmitter

In this section we consider a point magnetic dipole transmitter situated on the surface of a perfectly conducting metallic cylinder. The infinitely long cylinder with radius *a* is embedded in a homogeneous and isotropic lossy dielectric medium as shown in Figure 1.

A convergent integral representation, suitable for numerical computations, for the *z* component of the magnetic field valid at all points except for $z = 0$ on the surface of the cylinder is derived. The EM fields can be derived by solving Maxwell's equations directly or alternatively; they can be derived from derivatives of the Hertz magnetic vector potential [*Stratton*, 1941].

For a longitudinally oriented point magnetic dipole transmitter in the z direction, the Hertz vector is also in the z direction, i.e., $\Pi = (0, 0, \Pi_z)$, and satisfies the following partial differential equation (PDE) in cylindrical coordinates:

$$\frac{1}{r}\frac{\partial}{\partial r}\left(r\frac{\partial \Pi_z}{\partial r}\right) + \frac{1}{r^2}\frac{\partial^2 \Pi_z}{\partial \phi^2} + \frac{\partial^2 \Pi_z}{\partial z^2} + k^2 \Pi_z = \frac{-M_0 \delta(r - r_0)\delta(\phi)\delta(z)}{r}, \tag{1}$$

for the dipole transmitter located at (r_0,0,0), where, $r_0 \geq a$, a is the radius (in meters) of the "cylindrical pad," and $\delta(\cdot)$ are the well-known Dirac delta functions. Later we take the limit $r_0 \to a$ so that the transmitter is located on the cylinder surface. The boundary conditions and the solution to equation (1) are given in the following subsections.

2.1. Boundary Conditions

The EM fields outside of the source can be computed by differentiating the magnetic Hertz vector. The electric and magnetic fields are given by [*Stratton*, 1941]

$$\vec{E} = i\omega\mu_0 \nabla \times \vec{\Pi}, \tag{2}$$

and

$$\vec{H} = \nabla \times \nabla \times \vec{\Pi}. \tag{3}$$

The boundary conditions for a perfectly conducting cylinder require that the tangential electric fields vanish everywhere on the surface of the cylinder, i.e., $E_z = E_\phi = 0$ at $r = a$. From equation (2), $E_z = 0$ everywhere because $\vec{\Pi}$ has only a z component for a longitudinally oriented magnetic dipole transmitter in a homogeneous medium. This kind of EM wave is referred to as a transverse electric wave. From equation (2), the requirement that $E_\phi = 0$ at $r = a$ leads to the following boundary condition for the Hertz vector:

$$\frac{\partial \Pi_z}{\partial r} = 0, \text{ at } r = a. \tag{4}$$

In the next section equation (1) is solved subject to the boundary equation (4).

2.2. Solution of the PDE for the Hertz Vector

To solve the PDE in equation (1), it is useful to write Π_z in terms of the following integral transform:

$$\Pi_z(r, \phi, z) = \frac{2}{\pi}\sum_{n=0}^{\infty} \varepsilon_n \cos n\phi \int_0^\infty \Pi_n(r, \lambda) \cos \lambda z \, d\lambda, \tag{5}$$

where we have introduced the Neumann function $\varepsilon_n = \delta_{n,0} + 2(1 - \delta_{n,0})$, where $\delta_{n,0}$ is the Kronecker delta function so that $\varepsilon_0 = 1$ and $\varepsilon_n = 2$ for $n \geq 1$. The integral transform in equation (5) makes use of the fact that the Hertz vector (actually a scalar field in this case) is an even function of ϕ and z, which follows from the symmetry of the problem. If we substitute equation (5) into equation (1) we find that $\Pi_n(r, \lambda)$ obeys the modified Bessel function equation:

$$\frac{1}{r}\frac{d}{dr}\left(r\frac{d\Pi_n}{dr}\right) - \left[(\lambda^2 - k^2) + \frac{n^2}{r^2}\right]\Pi_n = \frac{-M_0 \delta(r - r_0)}{4\pi r}. \tag{6}$$

In arriving at equation (6) we made use of two well-known representations of the Dirac delta function:

$$\delta(\phi) = \frac{1}{2\pi}\sum_{n=0}^{\infty} \varepsilon_n \cos n\phi \tag{7a}$$

and

$$\delta(z) = \frac{1}{\pi}\int_0^\infty \cos \lambda z \, d\lambda. \tag{7b}$$

The general solution of equation (1) for $r < r_o$ can be written in terms of the modified Bessel functions K_n and I_n as

$$\Pi_n(\lambda, r) = A_n K_n(\gamma r) + \frac{M_o}{4\pi} K_n(\gamma r_o) I_n(\gamma r), \tag{8}$$

where we have defined the complex parameter, $\gamma = \sqrt{\lambda^2 - k^2}$. The first term in equation (8) is the solution of the homogeneous equation, which vanishes at infinity, and the second term satisfies the inhomogeneous

equation and is the interior ($r < r_o$) radial Green's function [*Jackson*, 1962]. The normalization factor multiplying the Green's function term in equation (8) is found by requiring that the solution has the correct discontinuity in its derivative at $r = r_o$. The discontinuity in the derivative is easily found from equation (6). The constants A_n are determined from the boundary condition in equation (4). Equations (4) and (8) are used to find that

$$A_n = -\frac{M_o}{4\pi}\frac{K_n(\gamma r_o) I_n'(\gamma a)}{K_n'(\gamma a)}. \tag{9}$$

Substituting equation (8) into equation (5) gives the following solution for the magnetic Hertz potential for a longitudinally oriented transmitter:

$$\Pi_z = \frac{2}{\pi}\sum_{n=0}^{\infty}\varepsilon_n \cos n\phi \int_0^{\infty}\left[A_n K_n(\gamma r) + \frac{M_o}{4\pi} K_n(\gamma r_0) I_n(\gamma r)\right]\cos \lambda z \, d\lambda, \tag{10}$$

with A_n given in equation (9). The next step is to compute the voltages induced in receivers situated on the cylindrical pad. For a longitudinally oriented dipole receiver the received signals are proportional to the z component of the magnetic field H_z evaluated at the receiver.

2.3. Solution for H_z Expressed as a Real Axis Integral

The z component of the magnetic field is computed from equation (3) by using the curl operator in cylindrical coordinates and recalling that $\vec{\Pi}$ has only a z component:

$$H_z = -\frac{1}{r}\frac{\partial}{\partial r}\left(r\frac{\partial \Pi_z}{\partial r}\right) - \frac{1}{r^2}\frac{\partial^2 \Pi_z}{\partial \phi^2}. \tag{11}$$

A simpler equation for H_z that is valid outside the source term can be obtained by combining equations (1) and (11):

$$H_z = \frac{\partial^2 \Pi_z}{\partial z^2} + k^2 \Pi_z. \tag{12}$$

Straightforward differentiations and combining of terms in equations (10) and (12) obtains the following real axis integral for H_z:

$$H_z = -\frac{1}{\pi}\sum_{n=0}^{\infty}\varepsilon_n \cos n\phi \int_{-\infty}^{\infty}\gamma^2\left[A_n K_n(\gamma r) + \frac{M_o}{4\pi} K_n(\gamma r_o) I_n(\gamma r)\right]\exp(i\lambda|z|)d\lambda. \tag{13}$$

In arriving at equation (13) we used the fact that the integrand is an even function of λ to extend the integral over the entire real axis and to write the cosine factor as a complex exponential. Also, we replaced the z coordinate by its absolute value which follows from the symmetry of the problem. The integrand in equation (13) can be simplified by recalling equation (9) for A_n and considering the two terms in square brackets. Simple algebra finds that these terms can be expressed in terms of the Wronskian of the modified Bessel functions, i.e.,

$$A_n K_n(\gamma a) + \frac{M_o}{4\pi} K_n(\gamma r_o) I_n(\gamma a) \equiv -\frac{M_o}{4\pi}\frac{K_n(\gamma r_o)}{K_n'(\gamma a)} W(K_n(\gamma a), I_n(\gamma a)), \tag{14}$$

where in arriving at equation (14) we have set $r_o = a$. We recall that the Wronskian for modified Bessel functions for all integer orders is

$$W(K_n(z), I_n(z)) = K_n(z) I_n'(z) - K_n'(z) I_n(z) = \frac{1}{z}. \tag{15}$$

The symbol z in equation (15) denotes a general complex variable. It is often used in this paper as the argument of Bessel functions in mathematical formulas such as Wronskians, asymptotic expansions, and recurrence formulas involving Bessel functions and should not be confused with the z coordinate of the cylindrical coordinate system.

Substituting equation (14) into equation (13) and using equation (15) leads to the following real axis integral for H_z:

$$H_z = \frac{M_o}{4\pi^2 a}\sum_{n=0}^{\infty}\varepsilon_n \cos n\phi \int_{-\infty}^{\infty}\gamma\frac{K_n(\gamma r_o)}{K_n'(\gamma a)}\exp(i\lambda|z|)\, d\lambda. \tag{16}$$

The real axis integral in equation (16) is a formal mathematical solution for the z component of the complex magnetic field everywhere on the surface of the cylindrical pad. It satisfies both the boundary conditions and

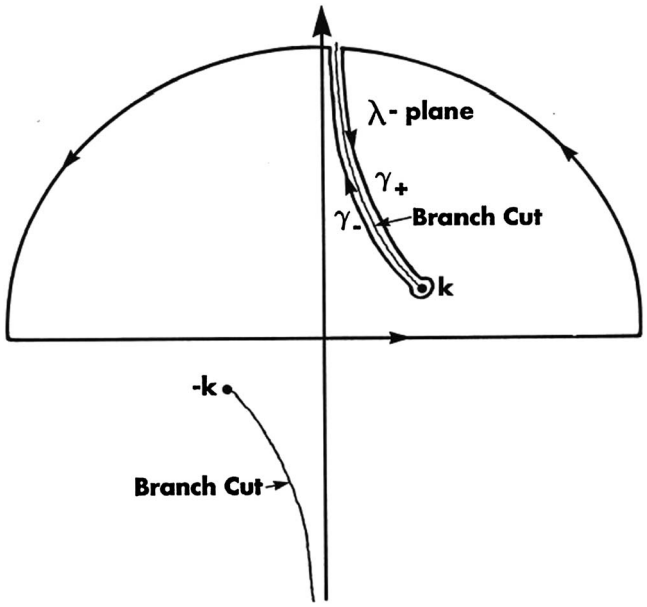

Figure 2. The contour and branch cut used to replace the poorly convergent real axis integrals for the magnetic fields in equations (18) and (81) with the convergent branch line integrals γ_+ and γ_- using Cauchy's theorem. On the branch cut, $\mathrm{Re}\gamma = 0$. The contour integration in the complex λ plane is performed on the upper Riemann sheet, where $\mathrm{Re}\gamma > 0$, for which the radiation condition is satisfied.

Maxwell's equations; however, it is not useful for computations because the real axis integral is poorly convergent. The integrand oscillates and increases linearly with λ for large values of λ when the transmitter is on the cylinder (i.e., when $r_o = a$). In the next section we use Cauchy's theorem and the contour in Figure 2 to replace the real axis integral by the sum of two convergent branch line integrals. It is easy to show that the integrand in equation (16) vanishes exponentially along the semicircular contour in the upper half λ plane for points off the real axis as the circular radius approaches infinity. This is clear for $|z| > 0$ if the contour in Figure 2 is used to perform the integration. The integrand must also vanish on the semicircular contour for $z = 0$ which is less obvious. The asymptotic behaviors of $K_n(\gamma r_o)$ and $K_n'(\gamma a)$ when $\gamma \to \infty$ (i.e., for $|\lambda| \to \infty$ on the semicircular contour) in equation (16) shows that the integrand behaves like $\gamma e^{-\gamma(r_o - a)}$ which goes to zero provided that $\mathrm{Re}\gamma > 0$. The latter condition is the radiation condition which requires that the fields vanish at infinity. The $\mathrm{Re}\,\gamma > 0$ requirement can also be shown from the asymptotic behavior, as $r \to \infty$ of the exterior Green's function (same as equation (8) if r and r_o are interchanged in the Green's function).

We can rewrite equation (16) using the well-known expression for the derivatives of modified Bessel functions of the second kind with integer order, i.e.,

$$K_n'(z) = -\frac{1}{2}(K_{n-1}(z) + K_{n+1}(z)), \tag{17}$$

where we note again that primes on Bessel functions in this paper denote differentiation with respect to their arguments. On substitution of equation (17) into equation (16),

$$H_z(a, \phi, z) = -\frac{M_o}{2\pi^2 a}\sum_{n=0}^{\infty}\varepsilon_n \cos n\phi \int_{-\infty}^{\infty}\left[\frac{\gamma K_n(\gamma r_o)}{K_{n-1}(\gamma a) + K_{n+1}(\gamma a)}\right]\exp(i\lambda|z|)d\lambda. \tag{18}$$

2.4. Derivation of a Convergent Integral for H_z

In this section we use Cauchy's theorem and the contour shown in Figure 2 to derive an exponentially convergent integral representation for H_z to replace the real axis integral in equation (18). Because $\gamma = \sqrt{\lambda^2 - k^2}$ is a double-valued function in the complex λ plane, the integrand has branch points at $\lambda = \pm k$. Cauchy's theorem requires that the integrand be analytic and single valued in the cut λ plane. This requires that there must be only one value of γ for each value of λ on the contour where the integration is performed. The sign of γ is fixed, and the integrand is single valued provided that the contour does not cross the branch cut in the complex λ plane in Figure 2 defined by $\mathrm{Re}\,\gamma = 0$. If the branch cut is crossed, the second Riemann sheet is passed to in the complex λ plane and the sign of γ changes. The complex λ plane therefore consists of two Riemann sheets that are joined by the branch cut on which $\mathrm{Re}\,\gamma = 0$. On the physical or upper sheet $\mathrm{Re}\,\gamma > 0$ and the radiation condition, i.e., the vanishing of the fields at an infinite distance from the transmitter is satisfied. Using Cauchy's theorem we can replace the real axis integral in equation (18) by the sum of the two branch line integrals around the branch cut. The reader might be concerned that the integrand in

equation (16) (or in equation (18)) has poles at the complex zeroes of $K_n'(\gamma a)$ and that the residues of these poles contribute to H_z. This would be unphysical because there can be no bound states or guided modes in an unbounded medium. Fortunately, there are no such modes because the zeroes of $K_n'(z)$ in the complex z plane are in the second and third quadrants for which the real parts of the complex zeroes are negative [*Kerimov and Skorokhodov*, 1984]. Therefore, zeroes of $K_n'(\gamma a)$ are present only on the unphysical Riemann sheet, where $\mathrm{Re}\,\gamma < 0$; therefore, these poles do not contribute to H_z. The contour integration in Figure 2 is performed on the physical sheet where $\mathrm{Re}\,\gamma > 0$.

The choice of the branch cut in Figure 2 leads to branch line integrals with integrands that decrease exponentially to zero as the dimensionless integration variable increases. Moreover, the Bessel functions in the integrands have real arguments which make possible very accurate numerical computations of the magnetic field. The branch cut is a hyperbola in the λ plane. This can easily be seen by first recalling that $\gamma^2 = \lambda^2 - k^2$. On writing the latter complex equation as separate equations for its real and imaginary parts and using the fact that $\mathrm{Re}\,\gamma = 0$ one finds from the equation for the imaginary part that $\lambda'\lambda'' = k'k''$, which are hyperbolas that start at $\lambda = \pm k$ in the complex λ plane. One can show from the equation for the real part of $\gamma^2 = \lambda^2 - k^2$ that the hyperbolas must asymptote to the vertical axis where $\lambda' = 0$. On the branch lines labeled γ_+ and γ_-, the complex parameter γ is purely imaginary and has the values

$$\gamma = \gamma_+ = u \exp\left(\frac{i\pi}{2}\right) \tag{19a}$$

and

$$\gamma = \gamma_- = u \exp\left(-\frac{i\pi}{2}\right). \tag{19b}$$

In the preceding equations u is a real coordinate variable ranging from ∞ to 0 on the branch line γ_+ and from 0 to ∞ on the branch line γ_-. The integrand is an analytic and single valued function (regular) in the cut λ plane. By Cauchy's theorem the following formula is obtained for H_z:

$$H_z(a, \phi, z) = -(I_+ + I_-), \tag{20}$$

where I_+ and I_- are the integrals along the branch lines and where we have made use of the facts that the integral along the semicircle vanishes as the radius goes to infinity and that the integrand has no poles on the physical Riemann sheet on which the integration is performed.

To calculate the branch line integrals we make use of the following formulas that relate modified Bessel functions of the second kind to Hankel functions. We use the following relations [*Olver*, 1965]:

$$K_n(z) = \frac{i\pi}{2} \exp\left(\frac{in\pi}{2}\right) H_n^{(1)}\left(z \exp\left(\frac{i\pi}{2}\right)\right) \qquad \left(-\pi < \arg z \le \frac{\pi}{2}\right) \tag{21a}$$

and

$$K_n(z) = -\frac{i\pi}{2} \exp\left(-\frac{in\pi}{2}\right) H_n^{(2)}\left(z \exp\left(-\frac{i\pi}{2}\right)\right) \qquad \left(-\frac{\pi}{2} < \arg z \le \pi\right). \tag{21b}$$

From these identities the functions $K_n(z)$ with pure imaginary arguments transform to Hankel functions with real arguments. To evaluate the branch line integral I_+ we first evaluate the modified Bessel function terms in the integrand of equation (18) on the branch line by recalling equation (19a) and using equation (21b):

$$\frac{K_n(\gamma a)}{\gamma(K_{n-1}(\gamma a) + K_{n+1}(\gamma a))} = \frac{K_n\left(ua \exp\left(\frac{i\pi}{2}\right)\right)}{\left(u \exp\left(\frac{i\pi}{2}\right)\right)\left(K_{n-1}\left(ua \exp\left(\frac{i\pi}{2}\right)\right) + K_{n+1}\left(ua \exp\left(\frac{i\pi}{2}\right)\right)\right)}, \tag{22}$$

$$= \frac{H_n^{(2)}(ua)}{u\left(H_{n+1}^{(2)}(ua) - H_{n-1}^{(2)}(ua)\right)}$$

where we set $r_o = a$ so that the transmitter is on the surface of the cylinder.

The Hankel functions of the second kind on the right-hand side of equation (22) are related to ordinary Bessel functions of the first and second kind:

$$H_n^{(2)}(ua) = J_n(ua) - iY_n(ua). \tag{23}$$

Using equation (22) and evaluating the integral in equation (18) on the branch line γ_+ results in

$$I_+ = -\frac{M_o}{2\pi^2 a}\sum_{n=0}^{\infty}\varepsilon_n \cos n\phi \int_0^{\infty} \frac{u^2 H_n^{(2)}(ua)\exp\left(i\sqrt{k^2-u^2}|z|\right)}{\sqrt{k^2-u^2}\left(H_{n+1}^{(2)}(ua) - H_{n-1}^{(2)}(ua)\right)}du, \tag{24}$$

where we have made the change of integration variables from λ to u using

$$d\lambda = -\frac{udu}{\sqrt{k^2-u^2}}. \tag{25}$$

The evaluation of the branch cut integral on γ_- in Figure 2 can easily be done in a similar manner by recalling equation (19b) and making use of equation (21a):

$$I_- = \frac{M_o}{2\pi^2 a}\sum_{n=0}^{\infty}\varepsilon_n \cos n\phi \int_0^{\infty} \frac{u^2 H_n^{(1)}(ua)\exp\left(i\sqrt{k^2-u^2}|z|\right)}{\sqrt{k^2-u^2}\left(H_{n+1}^{(1)}(ua) - H_{n-1}^{(1)}(ua)\right)}du, \tag{26}$$

where the Hankel functions of the first kind are

$$H_n^{(1)}(ua) = J_n(ua) + iY_n(ua), \tag{27}$$

which are complex conjugates of the Hankel functions of the second kind in equation (23).

Recalling equation (20) and using these results finds that

$$H_z = \frac{-iM_o}{2\pi^2 a}\sum_{n=0}^{\infty}\varepsilon_n \cos n\phi \int_0^{\infty} \frac{u^2 \exp\left(i\sqrt{k^2-u^2}|z|\right)}{\sqrt{k^2-u^2}} \mathrm{Im}\left[\frac{H_n^{(1)}(ua)}{H_n^{(1)\prime}(ua)}\right]du, \tag{28}$$

where Im[·] denotes the operation of taking the imaginary part of the expression in brackets, and we used the derivative relation

$$\left(H_n^{(1)}\right)' = \frac{1}{2}\left(H_{n-1}^{(1)} - H_{n+1}^{(1)}\right). \tag{29}$$

The integral for H_z converges exponentially for large values of the integration variable and can be used for computations in its present form. The Hankel function term in brackets in equation (28) can be simplified by further manipulations. To proceed, we take the imaginary part of the term in brackets after multiplying the numerator and denominator by the complex conjugate of the denominator which leads us to consider the following intermediate expression:

$$\frac{1}{2}\mathrm{Im}[\{(J_n(ua) + iY_n(ua)\} \times \{J_{n-1}(ua) - iY_{n-1}(ua) - J_{n+1}(ua) + iY_{n+1}(ua)\}] = -\frac{2}{\pi ua}, \tag{30}$$

where we used the following Bessel function Wronskian [*Olver*, 1965] relation valid for any complex variable z and for all integer orders:

$$W(J_n(z), Y_n(z)) \equiv J_n(z)Y_n'(z) - Y_n(z)J_n'(z) = \frac{2}{\pi z}. \tag{31}$$

Assembling these results we finally find the following compact and convergent solution for the z component of the magnetic field everywhere on the cylinder except for $z = 0$,

$$H_z(a, \phi, \bar{z}) = \frac{iM_o}{\pi^3 a^3}\sum_{n=0}^{\infty}\varepsilon_n \cos n\phi \int_0^{\infty} \frac{x\, G(x, ka, |\bar{z}|)}{\left|H_n^{(1)\prime}(x)\right|^2}dx, \tag{32}$$

where we define the dimensionless integration variable $x = ua$, the dimensionless z coordinate $|\bar{z}| = |z|/a$, and the function

$$G(x, ka, |\bar{z}|) = \frac{e^{i\sqrt{(ka)^2 - x^2}\,|\bar{z}|}}{\sqrt{(ka)^2 - x^2}}. \tag{33}$$

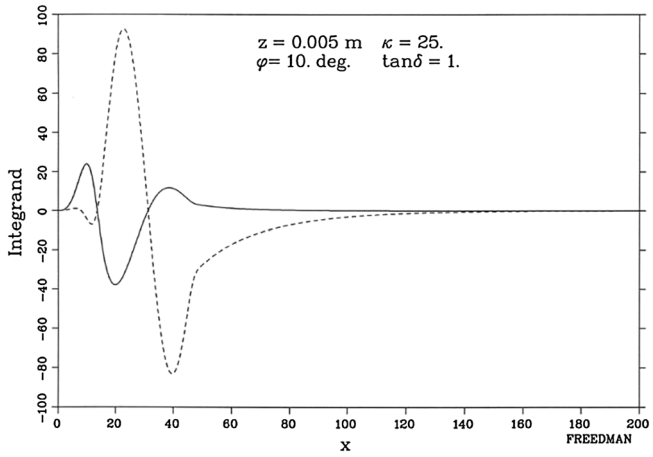

Figure 3. The real (solid) and imaginary (dashed) parts of the complex integrand in equation (32) plotted versus the dimensionless integration variable. The integrand is very smooth and decays rapidly to zero as the integration variable increases, a behavior that is typical for the integrands in equations (32) and (84). In this example, the receiver z coordinate was selected to be near (0.5 cm) the transmitter to show that the integrands decay quickly even for small z values. In practice, the transmitter-receiver distances are from about 3 to 12 cm. It was also found that at 1.1 GHz only 30 to 40 azimuthal modes (i.e., orders of the Hankel functions) in the summations were needed to achieve convergence of the integrands.

The integral in equation (32) is an exact and convergent integral representation for the z component of the complex frequency-dependent magnetic field everywhere on the cylinder surface except for $z=0$. Observe that the only complex quantity in the integrand in equation (32) is the function in equation (33). The constant factor multiplying the sum in equation (32) cancels when computing attenuations and phase shifts between receiver pairs because the latter quantities are computed from real and imaginary parts, respectively, of logarithms of the ratios of the complex magnetic field evaluated at the receiver positions [*Freedman and Vogiatzis*, 1979]. The real and imaginary parts of $H_z(a, \phi, z)$ can be accurately computed from equation (32) by using a simple numerical integration algorithm, e.g., Simpson's rule with automatic interval halving until convergence is achieved. For large values of x, the integrand decays to zero exponentially provided that $z \neq 0$; i.e., the transmitter and receiver are displaced from one another along the cylinder axis which is the case of practical interest. The integrand is computed for each value of the integration variable x by performing the summation in equation (32). The number of terms required in the summation increases with x and is problem dependent, but computations performed by the author typically required no more than 30 to 40 terms for computing the responses of a 1.1 GHz dielectric logging tool. The computations are both fast and accurate because the integrand is expressed in terms of Bessel functions with real arguments. The real and imaginary parts of the integrand in equation (32) are smooth functions of the integration variable x as shown in Figure 3 for a typical case. It is easy to show that the integrand vanishes for $x \to 0$ and for $x \to x_{\max}$ where $x_{\max}$ depends inversely on the z coordinate of the receiver.

3. Transversely Oriented Magnetic Dipole Transmitter

This section presents the detailed solution for a transversely oriented magnetic dipole transmitter situated on the surface of a perfectly conducting infinitely long cylinder situated in a lossy dielectric medium. As will become evident, this problem is more complex than that of the longitudinally oriented transmitter discussed in the previous section. The magnetic Hertz vector potential obeys the vector Helmholtz equation:

$$\nabla^2 \vec{\Pi} + k^2 \vec{\Pi} = -\frac{M_o \delta(r - r_o)\delta(\phi)\delta(z)}{r} \hat{\varepsilon}_\phi \tag{34}$$

for a point magnetic dipole transmitter at $(r_o,0,0)$ in cylindrical coordinates and oriented along the ϕ direction as indicated by the unit vector $\hat{\varepsilon}_\phi$ in equation (34). The vector operator $\vec{\nabla}^2$ in cylindrical coordinates [*Morse and Feshbach*, 1953] leads to coupled equations for Π_r and Π_ϕ; e.g., the two coupled PDEs are found from equation (34):

$$\nabla^2 \Pi_\phi - \frac{\Pi_\phi}{r^2} + \frac{2}{r^2}\frac{\partial \Pi_r}{\partial \phi} + k^2 \Pi_\phi = -\frac{M_o \delta(r - r_o)\delta(\phi)\delta(z)}{r} \tag{35}$$

and

$$\nabla^2 \Pi_r - \frac{\Pi_r}{r^2} - \frac{2}{r^2}\frac{\partial \Pi_\phi}{\partial \phi} + k^2 \Pi_r = 0. \tag{36}$$

As evident from the derivative terms in the two coupled equations that in order to satisfy the equations, Π_ϕ must be chosen as an even function of ϕ and Π_r as an odd function of ϕ. To proceed solutions of the form are assumed:

$$\Pi_\phi = \sum_{n=0}^{\infty} \varepsilon_n \cos n\phi \, \Pi_{\phi,n}(r,z) \tag{37}$$

and

$$\Pi_r = \sum_{n=0}^{\infty} \varepsilon_n \sin n\phi \, \Pi_{r,n}(r,z), \tag{38}$$

where we recall that $\varepsilon_0 = 1$ and $\varepsilon_n = 2$ for $n \geq 1$. It is convenient to define the operator ∇_R^2 as

$$\nabla_R^2 = \frac{1}{r}\frac{\partial}{\partial r}\left(r\frac{\partial}{\partial r}\right) + \frac{\partial^2}{\partial z^2}. \tag{39}$$

We then observe that

$$\nabla^2 = \nabla_R^2 + \frac{1}{r^2}\frac{\partial^2}{\partial \phi^2}, \tag{40}$$

and on substitution of equations (37) and (38) into equations (35) and (36),

$$\nabla_R^2 \Pi_{\phi,n} - \frac{(n^2+1)}{r^2}\Pi_{\phi,n} + \frac{2n}{r^2}\Pi_{r,n} + k^2 \Pi_{\phi,n} = -\frac{M_o \delta(r-r_o)\delta(z)}{2\pi r} \tag{41}$$

and

$$\nabla_R^2 \Pi_{r,n} - \frac{(n^2+1)}{r^2}\Pi_{r,n} + \frac{2n}{r^2}\Pi_{\phi,n} + k^2 \Pi_{r,n} = 0, \tag{42}$$

where in arriving at equation (41) we used a well-known representation for the Dirac delta function:

$$\delta(\phi) = \frac{1}{2\pi}\sum_{n=0}^{\infty} \varepsilon_n \cos n\phi. \tag{43}$$

To proceed, we introduce the cosine transform of $\widetilde{\Pi}_{\phi,n}$:

$$\Pi_{\phi,n}(r,z) = \frac{2}{\pi}\int_0^\infty \widetilde{\Pi}_{\phi,n}(r,\lambda)\cos\lambda z \;\; d\lambda, \tag{44}$$

and the inverse

$$\widetilde{\Pi}_{\phi,n}(r,\lambda) = \int_0^\infty \Pi_{\phi,n}(r,z)\cos\lambda z \;\; dz, \tag{45}$$

and similar cosine transform equations for $\Pi_{r,n}$ which are not displayed here to save space. Upon taking the cosine transform of equation (41) and using a well-known representation for the Dirac delta function,

$$\delta(z) = \frac{1}{\pi}\int_0^\infty \cos\lambda z \, d\lambda, \tag{46}$$

and we find the following:

$$\frac{1}{r}\frac{\partial}{\partial r}\left(r\frac{\partial \widetilde{\Pi}_{\phi,n}}{\partial r}\right) - \left(\lambda^2 + \frac{n^2+1}{r^2}\right)\widetilde{\Pi}_{\phi,n} + \frac{2n}{r^2}\widetilde{\Pi}_{r,n} + k^2\widetilde{\Pi}_{\phi,n} = -\frac{M_o\delta(r-r_o)}{4\pi r}. \tag{47}$$

Taking the cosine transform of equation (42) obtains

$$\frac{1}{r}\frac{\partial}{\partial r}\left(r\frac{\partial \widetilde{\Pi}_{r,n}}{\partial r}\right) - \left(\lambda^2 + \frac{n^2+1}{r^2}\right)\widetilde{\Pi}_{r,n} + \frac{2n}{r^2}\widetilde{\Pi}_{\phi,n} + k^2\widetilde{\Pi}_{r,n} = 0. \tag{48}$$

The next step is to introduce the sum and the difference of the potentials $\widetilde{\Pi}_{\phi,n}$ and $\widetilde{\Pi}_{r,n}$, which leads to a pair of uncoupled equations. The sum and difference potentials are defined, respectively, by

$$\widetilde{\Pi}_{S,n}(r,\lambda) = \widetilde{\Pi}_{\phi,n}(r,\lambda) + \widetilde{\Pi}_{r,n}(r,\lambda) \tag{49}$$

and

$$\widetilde{\Pi}_{D,n}(r,\lambda) = \widetilde{\Pi}_{\phi,n}(r,\lambda) - \widetilde{\Pi}_{r,n}(r,\lambda). \tag{50}$$

Adding equations (47) and (48) results in

$$\frac{1}{r}\frac{\partial}{\partial r}\left(r\frac{\partial\widetilde{\Pi}_{S,n}}{\partial r}\right)-\left(\lambda^2+\frac{(n-1)^2}{r^2}\right)\widetilde{\Pi}_{S,n}+k^2\widetilde{\Pi}_{S,n}=-\frac{M_o\delta(r-r_o)}{4\pi r}, \tag{51}$$

and subtracting the equations gives

$$\frac{1}{r}\frac{\partial}{\partial r}\left(r\frac{\partial\widetilde{\Pi}_{D,n}}{\partial r}\right)-\left(\lambda^2+\frac{(n+1)^2}{r^2}\right)\widetilde{\Pi}_{D,n}+k^2\widetilde{\Pi}_{D,n}=-\frac{M_o\delta(r-r_o)}{4\pi r}. \tag{52}$$

The homogeneous equations (51) and (52) are satisfied by modified Bessel functions valid in the domain $a\le r\le\infty$. The inhomogeneous equations are satisfied by the interior radial Green's functions. The general solutions for $r<r_o$ that vanish at infinity are

$$\widetilde{\Pi}_{S,n}=A_n K_{n-1}(\gamma r)+\frac{M_o}{4\pi}K_{n-1}(\gamma r_o)\,I_{n-1}(\gamma r) \tag{53}$$

and

$$\widetilde{\Pi}_{D,n}=B_n K_{n+1}(\gamma r)+\frac{M_o}{4\pi}K_{n+1}(\gamma r_o)\,I_{n+1}(\gamma r), \tag{54}$$

where the coefficients A_n and B_n are determined from the boundary conditions on the EM fields. The second term in each of these two equations consist of interior radial Green's functions and $\gamma=\sqrt{\lambda^2-k^2}$. The factor multiplying the Green's function is determined by the discontinuity in the derivative of the Green functions at $r=r_o$ which can be computed from equations (51) and (52). Note that $\widetilde{\Pi}_{\phi,n}$ and $\widetilde{\Pi}_{r,n}$ can be computed from equations (53) and (54) using equations (49) and (50). First, however we must determine the coefficients A_n and B_n in the preceding equations by using the boundary conditions satisfied by the EM fields.

3.1. Boundary Conditions

The boundary conditions require that the tangential components of the electric field E_z and E_ϕ vanish on the surface of the perfectly conducting cylinder for $r=a$:

$$\left(\nabla\times\vec{\Pi}\right)\cdot\widehat{\varepsilon_z}=0 \tag{55a}$$

and

$$\left(\nabla\times\vec{\Pi}\right)\cdot\widehat{\varepsilon_\phi}=0, \tag{55b}$$

where we recall that $\vec{\Pi}=\left(\Pi_r,\Pi_\phi,0\right)$, which leads for $E_z=0$ to

$$\left(\frac{\partial\Pi_\phi}{\partial r}+\frac{\Pi_\phi}{r}-\frac{1}{r}\frac{\partial\Pi_r}{\partial\phi}\right)_{r=a}=0, \tag{56}$$

and $E_\phi=0$ leads to

$$\left(\frac{\partial\Pi_r}{\partial z}\right)_{r=a}=0. \tag{57}$$

The boundary condition equations can be written in terms of the cosine transforms of the Hertz potentials by recalling equation (44) and the analogous cosine transform for Π_r. Equation (56) then leads to

$$\left(\frac{\partial\widetilde{\Pi}_{\phi,n}}{\partial r}+\frac{\widetilde{\Pi}_{\phi,n}}{r}\right)_{r=a}=0 \tag{58a}$$

And the boundary condition in equation (57) leads to

$$\widetilde{\Pi}_{r,n}(a,\lambda)=0. \tag{58b}$$

The term that has the derivative of $\widetilde{\Pi}_r$ in equation (56) is not present in equation (58a) because it vanishes by virtue of equation (58b). These boundary condition equations are used to determine the coefficients A_n and

B_n in equations (53) and (54). However, to proceed we first must write the boundary conditions in terms of the sum and difference potentials. Recalling that

$$\widetilde{\Pi}_{\phi,n} = \frac{\widetilde{\Pi}_{S,n} + \widetilde{\Pi}_{D,n}}{2} \tag{59}$$

and

$$\widetilde{\Pi}_{r,n} = \frac{\widetilde{\Pi}_{S,n} - \widetilde{\Pi}_{D,n}}{2}. \tag{60}$$

It is easily found from equations (58a), (58b), (59), and (60) that

$$\widetilde{\Pi}_{S,n}(a,\lambda) = \widetilde{\Pi}_{D,n}(a,\lambda) \tag{61a}$$

and

$$\left(\frac{\partial\left(\widetilde{\Pi}_{S,n} + \widetilde{\Pi}_{D,n}\right)}{\partial r} + \frac{\left(\widetilde{\Pi}_{S,n} + \widetilde{\Pi}_{D,n}\right)}{a}\right)_{r=a} = 0. \tag{61b}$$

Performing some straightforward but tedious algebra on the boundary condition in equation (61b) after recalling equations (53) and (54) results in

$$A_n K_n(\gamma a) + B_n K_n(\gamma a) = \frac{M_o}{4\pi} I_n(\gamma a)(K_{n-1}(\gamma r_o) + K_{n+1}(\gamma r_o)), \tag{62}$$

and from the boundary condition in equation (61a) it is easily found that

$$A_n K_{n-1}(\gamma a) - B_n K_{n+1}(\gamma a) = \frac{M_o}{4\pi}(K_{n+1}(\gamma r_o) I_{n+1}(\gamma a) - K_{n-1}(\gamma r_o) I_{n-1}(\gamma a)). \tag{63}$$

In deriving equation (62), we made use of the following useful relations for derivatives of modified Bessel functions [*Olver*, 1965]:

$$K'_{n+1}(z) = -K_n(z) - \frac{n+1}{z} K_{n+1}(z), \tag{64a}$$

$$K'_{n-1}(z) = -K_n(z) + \frac{n-1}{z} K_{n-1}(z), \tag{64b}$$

$$I'_{n+1}(z) = I_n(z) - \frac{n+1}{z} I_{n+1}(z), \tag{64c}$$

and

$$I'_{n-1}(z) = I_n(z) + \frac{n-1}{z} I_{n-1}(z). \tag{64d}$$

The coefficients A_n and B_n in equations (53) and (54) are found by solving equations (62) and (63). After considerable algebra we can write the solutions in the following form:

$$A_n = \frac{M_o I_{n-1}(\gamma a)}{4\pi} + \frac{M_o}{2\pi\gamma a} \frac{K_{n+1}(\gamma a)}{K_n(\gamma a)(K_{n+1}(\gamma a) + K_{n-1}(\gamma a))} \tag{65}$$

and

$$B_n = \frac{M_o I_{n+1}(\gamma a)}{4\pi} + \frac{M_o}{2\pi\gamma a} \frac{K_{n-1}(\gamma a)}{K_n(\gamma a)(K_{n+1}(\gamma a) + K_{n-1}(\gamma a))}. \tag{66}$$

In arriving at these equations we have set $r_o = a$, so that the point magnetic dipole transmitter is on the surface of the cylinder. We also used some well-known Bessel function Wronskian equations, i.e.,

$$K_{n-1}(\gamma a) I_n(\gamma a) + K_n(\gamma a) I_{n-1}(\gamma a) = \frac{1}{\gamma a} \tag{67a}$$

and

$$K_{n+1}(\gamma a) I_n(\gamma a) + K_n(\gamma a) I_{n+1}(\gamma a) = \frac{1}{\gamma a}. \tag{67b}$$

In the next section we use the results of the preceding two sections to derive a convergent integral representation for $H_\phi(a, \phi, z)$ that is valid everywhere on the cylinder except for $z = 0$.

3.2. Calculation of Real Axis Integral for $H_\phi(a, \phi, z)$

We recall that the magnetic field can be computed from the equation $\vec{H} = \nabla\times\nabla\times\vec{\Pi}$, so that in cylindrical coordinates:

$$H_\phi = -\frac{\partial^2\Pi_\phi}{\partial r^2} - \frac{1}{r}\frac{\partial\Pi_\phi}{\partial r} + \frac{\Pi_\phi}{r^2} - \frac{\partial^2\Pi_\phi}{\partial z^2} - \frac{1}{r^2}\frac{\partial\Pi_r}{\partial\phi} + \frac{1}{r}\frac{\partial^2\Pi_r}{\partial r\partial\phi}. \tag{68}$$

The complicated expression in equation (68) can be simplified by using the homogeneous equation (34) satisfied by the Hertz vector outside of the source to reduce to the simpler form

$$H_\phi(a, \phi, z) = k^2\Pi_\phi + \frac{1}{a^2}\frac{\partial^2\Pi_\phi}{\partial\phi^2} + \frac{1}{a}\frac{\partial^2\Pi_r}{\partial r\partial\phi}. \tag{69}$$

The term with the first-order derivative of Π_r with respect to ϕ in equation (68) does not contribute to $H_\phi(a, \phi, z)$ because it vanishes from the boundary condition in equation (58b). Recalling equations (37), (38), (44), (53), (54), (59), and (60) we used equation (69) to find

$$H_\phi(a, \phi, z) = \frac{1}{\pi}\sum_{n=0}^{\infty}\varepsilon_n\left(k^2 - \frac{n^2}{a^2}\right)\cos n\phi\int_0^\infty\left\{\left[A_n + \frac{M_o}{4\pi}I_{n-1}(\gamma a)\right]K_{n-1}(\gamma a) + \left[B_n + \frac{M_o}{4\pi}I_{n+1}(\gamma a)\right]K_{n+1}(\gamma a)\right\}\cos\lambda z\, d\lambda$$
$$+ \frac{1}{\pi}\sum_{n=0}^{\infty}\varepsilon_n\frac{n}{a}\cos n\phi\int_0^\infty\left\{\gamma\left[A_nK'_{n-1}(\gamma a) + \frac{M_o}{4\pi}K_{n-1}(\gamma a)I'_{n-1}(\gamma a)\right] - \gamma\left[B_nK'_{n+1}(\gamma a) + \frac{M_o}{4\pi}K_{n+1}(\gamma a)I'_{n+1}(\gamma a)\right]\right\}\cos\lambda z\, d\lambda. \tag{70}$$

Equation (70) can be simplified as follows. The above integral is conveniently written as

$$H_\phi = \frac{1}{\pi}\sum_{n=0}^{\infty}\varepsilon_n\cos n\phi\int_0^\infty(T_{1n}(\lambda) + T_{2n}(\lambda))\cos\lambda z\, d\lambda, \tag{71}$$

and recalling equations (53) and (54) finds that

$$T_{1n} = \left(k^2 - \frac{n^2}{a^2}\right)\cdot\left(\widetilde{\Pi}_{Sn} + \widetilde{\Pi}_{Dn}\right). \tag{72}$$

The second term in equation (71) is more complicated. It is the sum of two terms, i.e.,

$$T_{2n} = \frac{n\gamma}{a}\left[A_nK'_{n-1}(\gamma a) + \frac{M_o}{4\pi}K_{n-1}(\gamma a)I'_{n-1}(\gamma a)\right] - \frac{n\gamma}{a}\left[B_nK'_{n+1}(\gamma a) + \frac{M_o}{4\pi}K_{n+1}(\gamma a)I'_{n+1}(\gamma a)\right]. \tag{73}$$

Equations (64a)–(64d) are used for the derivatives of the Bessel functions to find after some algebra that

$$T_{2n} = \frac{n\gamma}{a}\left[\frac{n}{\gamma a}\left[\widetilde{\Pi}_{Sn}(\gamma a) + \widetilde{\Pi}_{Dn}(\gamma a)\right] - (A_n - B_n)\cdot K_n(\gamma a) + \frac{M_0}{4\pi}I_n(\gamma a)\cdot[K_{n-1}(\gamma a) - K_{n+1}(\gamma a)]\right]. \tag{74}$$

Then, equations (72) and (74) are added:

$$T_{1n} + T_{2n} = -\frac{n\gamma}{a}K_n(\gamma a)\left[(A_n - B_n) + \frac{nM_0I_n(\gamma a)}{2\pi\gamma a}\right] + k^2\left(\widetilde{\Pi}_{Sn} + \widetilde{\Pi}_{Dn}\right), \tag{75}$$

where in arriving at equation (75) we made use of the recurrence relation for the modified Bessel functions K_n [*Olver*, 1965]:

$$K_{n+1}(\gamma a) - K_{n-1}(\gamma a) = \frac{2n}{\gamma a}K_n(\gamma a). \tag{76}$$

Finally, equations (65) and (66) are used to simplify the term in brackets in equation (75):

$$A_n - B_n + \frac{nM_0I_n(\gamma a)}{2\pi\gamma a} = \frac{nM_0}{\pi(\gamma a)^2(K_{n+1}(\gamma a) + K_{n-1}(\gamma a))}, \tag{77}$$

where we used equation (76) and a similar recurrence relation for the modified Bessel functions I_n:

$$I_{n+1}(\gamma a) - I_{n-1}(\gamma a) = -\frac{2n}{\gamma a}I_n(\gamma a). \tag{78}$$

The last term in equation (75) can also be simplified by using equations (53), (54), (65), and (66):

$$\widetilde{\Pi}_{Sn} + \widetilde{\Pi}_{Dn} = \frac{M_0}{\pi\gamma a} \frac{K_{n-1}(\gamma a)K_{n+1}(\gamma a)}{K_n(\gamma a)[K_{n+1}(\gamma a) + K_{n-1}(\gamma a)]}. \tag{79}$$

Assembling these results and combining terms gives

$$T_{1n} + T_{2n} = \frac{M_0}{\pi\gamma a^3} \frac{\left[(ka)^2 K_{n-1}(\gamma a)K_{n+1}(\gamma a) - n^2 K_n^2(\gamma a)\right]}{K_n(\gamma a)[K_{n+1}(\gamma a) + K_{n-1}(\gamma a)]}, \tag{80}$$

which on substitution into equation (71) leads to the following real axis integral solution:

$$H_\phi(a, \phi, z) = \frac{M_0}{2\pi^2 a^2} \sum_{n=0}^{\infty} \varepsilon_n \cos n\phi \int_{-\infty}^{\infty} \frac{\left[(ka)^2 K_{n-1}(\gamma a)K_{n+1}(\gamma a) - n^2 K_n^2(\gamma a)\right] \exp(i\lambda|z|)}{(\gamma a)K_n(\gamma a)[K_{n+1}(\gamma a) + K_{n-1}(\gamma a)]}\, d\lambda. \tag{81}$$

The extra factor of 2 multiplying the sum in equation (81) comes from noting that the integrand is an even function of λ and extending the limits of the integral to cover the entire real axis. We also replaced z in the exponential with $|z|$ because it follows from the symmetry of the problem that the magnetic field is an even function of z. Similar to the real axis integral for $H_z(a, \phi, z)$ in equation (18) the integrand in equation (81) is oscillatory and poorly convergent for large λ so it is not useful for numerical computations. Following similar arguments to those in section 2.4, the integral in equation (81) has branch points in the complex λ plane at $\lambda = \pm k$ and the integral can be replaced by the sum of two convergent branch line integrals using Cauchy's theorem and the contour in Figure 2. The integrand in equation (81) has no poles on the physical Riemann sheet because the zeroes of both $K_n(z)$ and $K_n'(z)$ in the complex z plane are in the second and third quadrants so the real parts of the complex roots are negative. Therefore, the zeroes of the functions $K_n(\gamma a)$ and $K_n'(\gamma a)$ (the factor in brackets) in the denominator of the integrand in equation (81) occur only on the unphysical Riemann sheet, where $\mathrm{Re}\,\gamma < 0$. The contour integration in Figure 2 is performed on the physical Riemann sheet, where $\mathrm{Re}\,\gamma > 0$, for which the radiation condition is satisfied.

3.3. Derivation of a Convergent Integral for H_ϕ

The real axis integral in equation (81) can be transformed into the sum of two convergent branch line integrals using the same contour shown in Figure 2. It is easy to show that the integrand vanishes everywhere on the semicircle as its radius approaches infinity and that the integral on the circle around the branch point vanishes as the radius of the circle approaches zero. The two branch line integrals I_+ and I_- can be evaluated following the same procedure used in section 2.4. Recalling equations (19a), (21b), and (25) and applying some algebra results in

$$I_+ = \frac{M_0}{2\pi^2 a^3} \sum_{n=0}^{\infty} \varepsilon_n \cos n\phi \int_0^{\infty} \frac{\left[(ka)^2 H_{n-1}^{(2)}(x)H_{n+1}^{(2)}(x) - n^2\left(H_n^{(2)}(x)\right)^2\right] G(x, ka, |\bar{z}|)}{H_n^{(2)}(x)\left(H_{n+1}^{(2)}(x) - H_{n-1}^{(2)}(x)\right)}\, dx, \tag{82}$$

where we have introduced the dimensionless integration variable $x = ua$, defined the normalized z coordinate $|\bar{z}| = |z|/a$ and recalled the function $G(x, ka, |\bar{z}|)$, which was defined in equation (33). The Hankel functions of the second kind are defined in equation (23). For large values of the integration variable the integrand vanishes exponentially provided that $z \neq 0$. The branch line integral I_- is also easily performed by using the transformation in equation (19b) and also using equation (21a). Applying some algebra yields

$$I_- = -\frac{M_0}{2\pi^2 a^3} \sum_{n=0}^{\infty} \varepsilon_n \cos n\phi \int_0^{\infty} \frac{\left[(ka)^2 H_{n-1}^{(1)}(x)H_{n+1}^{(1)}(x) - n^2\left(H_n^{(1)}(x)\right)^2\right] G(x, ka, |\bar{z}|)}{H_n^{(1)}(x)\left(H_{n+1}^{(1)}(x) - H_{n-1}^{(1)}(x)\right)}\, dx. \tag{83}$$

Because the integrand in equation (81) is a regular function of λ in the cut λ plane and has no poles, we can use the contour in Figure 2 and Cauchy's theorem (e.g., see equation (20)) to express the real axis integral in equation (81) as the sum of the two branch line integrals in equations (82) and (83). These equations add to

$$H_\phi(a, \phi, z) = \frac{i M_o}{2\pi^2 a^3} \sum_{n=0}^{\infty} \varepsilon_n \cos n\, \phi \int_0^{\infty} G(x, ka, |\bar{z}|) \cdot \left[(ka)^2 U_n(x) - n^2 V_n(x)\right] dx, \tag{84}$$

where we have defined the functions

$$U_n(x) = \frac{\mathrm{Im}\left[H_{n-1}^{(2)}(x)\cdot H_{n+1}^{(2)}(x)\cdot H_n^{(1)}(x)\cdot H_n^{(1)\prime}(x)\right]}{\left|H_n^{(1)}(x)\right|^2\cdot\left|H_n^{(1)\prime}(x)\right|^2}, \tag{85}$$

$$V_n(x) = \frac{\mathrm{Im}\left[\left(H_n^{(2)}(x)\right)^2\cdot H_n^{(1)}(x)\cdot H_n^{(1)\prime}(x)\right]}{\left|H_n^{(1)}(x)\right|^2\cdot\left|H_n^{(1)\prime}(x)\right|^2}. \tag{86}$$

The dot symbol denotes ordinary scalar multiplication, and Im[ ] denotes the operation of taking the imaginary part of the complex quantity in brackets. The primes are derivatives of the Hankel functions with respect to their arguments.

The integral in equation (84) is an exact and convergent integral representation for the ϕ component of the complex frequency-dependent magnetic field, and it is convergent everywhere on the cylinder surface except for $z = 0$. The only complex quantity in the integrand in equation (84) is the function $G(x, ka, |\bar{z}|)$ defined in equation (33). The real and imaginary parts of $H_\phi(a, \phi, z)$ can be computed accurately from equation (84) by using any numerical integration algorithm, e.g., Simpson's rule with automatic interval halving until convergence is achieved. For large values of x, the integrand decays to zero exponentially provided that $z \neq 0$, i.e., for the transmitter and receiver displaced from one another along the cylinder axis which is the case of practical interest. The integrand is computed for each value of the integration variable x by performing the summation in equation (84). The number of terms required in the summation generally increases with x and is problem dependent, but computations performed by the author typically required no more than 30 to 40 terms for computing the responses of a 1.1 GHz dielectric logging tool. The computations are fast and accurate because the integrand is expressed in terms of Bessel functions with real arguments. It is easy to show that the integrand in equation (84) has an integrable singularity as $x \to 0$. The singularity comes from the small x behavior of the $n = 0$ term enclosed in brackets in equation (84). This poses no problems for the accuracy of the numerical integration because for small x the integral can be done analytically, and this contribution (negligible for sufficiently small values of $x_{\min}$) can be added to the numerical integration in the interval from $x_{\min}$ to $x_{\max}$. The upper limit $x_{\max}$ of the integral is determined by choosing a value of the integration variable for which the integrand has decayed to a negligibly small value.

4. Conclusions

New and exact integral representations were derived in this paper for complex magnetic fields on a metal cylinder excited by longitudinal and transverse oscillating magnetic dipoles on the cylinder surface. These solutions are useful for performing accurate computations for problems of interest in EM well logging. The computational details and results should also be of interest to scientists and engineers working on academic, industrial, and military EM problems.

Acknowledgments

It is a pleasure to thank J.P. Vogiatzis for many productive lunchtime discussions during the course of this work. I also thank W.C. Chew for his instructive comments at a seminar I presented on these calculations at the University of Illinois and V. Druskin at the Schlumberger-Doll Research Center for a productive discussion during the writing of this paper. I also owe thanks to Schlumberger management for permission to publish this work.

References

Chew, W. C. (1988), Modeling of the dielectric logging tool at high frequencies: Theory, *IEEE Trans. Geosci. Remote Sens.*, *26*(4), 382–387, doi:10.1109/36.3041.

Chew, W. C., and S. C. Gianzero (1981), Theoretical investigation of the electromagnetic wave propagation tool, *IEEE Trans. Geosci. Remote Sens.*, *GE-19*(1), 1–7, doi:10.1109/tgrs.1981.350321.

Freedman R. (1992), Method and apparatus for measuring azimuthal as well as longitudinal waves in a formation traversed by a borehole, U.S. Patent 5 168 234, 1 Dec.

Freedman, R., and J. P. Vogiatzis (1979), Theory of microwave dielectric logging using the electromagnetic wave propagation method, *Geophysics*, *44*(5), 969–986, doi:10.1190/1.1441048.

Jackson, J. D. (1962), Boundary-value problems in electrostatics: II, in *Classical Electrodynamics*, pp. 85–86, Wiley, New York.

Kerimov, M. K., and S. L. Skorokhodov (1984), Calculation of the complex zeroes of the modified Bessel function of the second kind and its derivatives, *USSR Comput. Math. Math. Phys.*, *24*(4), 115–123, doi:10.1016/0041-5553(84)90243-x.

Morse, P. M., and H. Feshbach (1953), Types of fields, in *Methods of Theoretical Physics Part I*, 1st ed., chap. 1–8, pp. 115–116, McGraw-Hill, New York.

Olver, F. W. J. (1965), Bessel functions of integer order, in *Handbook of Mathematical Functions*, edited by M. Abramowitz and I. A. Stegun, pp. 358–433, Dover, New York.

Sayfina, K., T. Habashy, C. Randall, B. Clark, and A. Perez-Falcon (1987), Experimental and theoretical study of electromagnetic propagation tool in layered and homogeneous media, *SPE Form. Eval.*, *2*(3), 289–302, doi:10.2118/14188-PA.

Stratton, J. A. (1941), The electromagnetic potentials, in *Electromagnetic Theory*, pp. 23–32, McGraw-Hill, New York.

Wait, J. R. (1987), General solution for excitation by slotted aperture source in conducting cylinder with concentric layering, *IEEE Trans. Microwave Theory Tech.*, *35*(3), 321–325, doi:10.1109/TMTT.1987.1133645.

Erratum

In the originally published version of this article, the title was lacking a Roman numeral I to indicate that it is the first part of a multi-part series. The error has since been corrected and this version may be considered the authoritative version of record.